PAPER

Many-body effects and non-local charge fluctuations in the double perovskite Sr₂FeMoO₆

Henrique P. Martins, [ID] *[a] Eduardo B. Guedes,[a] Rodrigo J. O. Mossanek,[a] Fernando D. Prado,[b] Alberto Caneiro[c] and Miguel Abbate[a]

We studied the electronic structure of Sr_2FeMoO_6 using core level and valence band photoemission. The spectra were obtained using high energy X-rays of 1840 eV, which provide bulk sensitive information on the electronic structure. The experimental data were analyzed using the spectral weight from cluster model calculations. The ground state reveals a large Fe–O and Mo–O hybridization, as well as the importance of non-local Fe–O–Mo charge fluctuations. The latter is crucial to explain the half-metallic character attributed to the Sr_2FeMoO_6 compound. The core level and valence band photoemission spectra show charge transfer satellites. These satellites are related to many-body effects and are larger for the Fe levels than for the Mo states.

1   Introduction

The Sr_2FeMoO_6 (SFMO) double perovskite presents very interesting physical properties.[1,2] The crystal structure of this compound is tetragonal with $a = 5.557$ Å and $c = 7.887$ Å. This material is a half-metallic ferrimagnet with an ordering temperature of $T_C = 420$ K. The magnetic moment, up to $\mu = 3.7$ μ_B, depends on the degree of Fe/Mo cationic disorder.[3] The SFMO oxide exhibits a considerable magneto-resistance (MR) at room temperature. The accepted MR mechanism involves tunneling across grain boundaries. For these reasons, this compound is being considered for applications in spintronic devices. More details on the SFMO double perovskite can be found in recent reviews.[4–6]

The electronic structure of SFMO was studied using a variety of spectroscopic techniques, which aimed at understanding the microscopic origin of its physical properties.[7] The optical conductivity confirmed the half-metallic character of the SFMO compound.[2] The core-level X-ray photoelectron spectra (XPS) determined the chemical shifts of the Fe/Mo ions.[8,9] The valence band X-ray photoemission spectra (PES) elucidated the electronic states at the Fermi level.[10–12] The X-ray absorption spectra (XAS) was utilized to investigate the Fe/Mo valencies.[9,11,13] The X-ray emission spectra (XES) provided site selected information on the electronic structure.[14] Finally, the magnetic circular dichroism spectra (MCD) was used to study the Fe/Mo magnetic moments.[13,15]

a Departamento de Física, Universidade Federal do Paraná, Caixa Postal 19044, 81531-990 Curitiba, PR, Brazil. E-mail: hpmartins@gmail.com

b Departamento de Física, Universidad Nacional del Sur, Av. Leandro N. Alem 1253, 8000 Bahía Blanca, Argentina

c Centro Atómico Bariloche, Comisión Nacional de Energía Atómica, Av. Ezequiel Bustillo 9500, 8400 Bariloche, Argentina

In an ionic approximation, the electronic structure of SFMO can be viewed as a combination of Fe^{3+} ($3d^5$) and Mo^{5+} ($4d^1$).[1,2] However, the Fe 3d and Mo 4d electrons present a covalent hybridization with the O 2p states.[12] Further, the majority Fe^{3+} ($3d^5$) electrons are localized, whereas the minority Mo^{5+} ($4d^1$) electron is itinerant, which is consistent with both the half-metallic conductivity and the ferrimagnetic ordering of SFMO. In fact, the conducting electron is delocalized along Mo–O–Fe–O–Mo chains in this material, indicating the importance of the Fe 3d–O 2p and Mo 4d–O 2p covalent mixing, as well as the non-local Mo–O–Fe charge fluctuations.

The valence band spectra of SFMO were compared to diverse density functional theory (DFT) methods. The agreement with the experiment improves if one includes in the calculation the Mott–Hubbard U.[10,11] The values of U used in the LDA + U approach at the Fe sites are relatively large, about $U = 2$–4 eV. Based on these values, Kuepper *et al.* concluded that the electronic structure of SFMO was highly correlated.[14] In particular, the valence band spectra of this oxide might present distinct many-body effects beyond the DFT description.

We studied the electronic structure of SFMO using a cluster model approach,[16–19] which consists of two FeO_6 and MoO_6 octahedra which are either connected (double cluster model) or not (single cluster model) by one corner O atom. This method includes both the Fe 3d–O 2p and Mo 4d–O 2p hybridization, as well as the Mo–O–Fe charge fluctuations in the FeO_6–MoO_6 double cluster. The electronic structure is calculated using the configuration interaction approach,[17] which includes many relevant correlation effects within the double cluster. The calculations are compared to the core level and valence band spectra of SFMO. Finally, the experimental spectra were obtained using bulk sensitive high-energy X-rays.

2 Experimental details

The ceramic Sr_2FeMoO_6 sample was prepared using the solid-state reaction method. The corresponding reagents were mixed and calcined in air at 950 °C for 24 h. The resulting powder was pulverized, mixed and fired again several times. The reduction of the powder was carried out in a flowing mixture of 1% H_2–Ar gas at 1050 °C for 1 h. Finally, the substance was ground, pressed into pellets, and sintered in a vacuum for 12 h at 1200 °C. The powder XRD analysis confirmed that the sample was a single-phase material. The Rietveld refinement showed a tetragonal $I4/mmm$ structure with the aforementioned parameters. The relative intensity of the (101) reflection indicated a highly ordered sample with less than 3% cationic disorder.[3]

The photoemission measurements were performed at the SXS beamline at the Laboratório Nacional de Luz Síncrotron (LNLS) in Campinas (Brazil).[20] The photon energy scale of the monochromator was calibrated using the Si K absorption edges. The photoemission spectra was taken using a SPECS Phoibos 150 electron energy analyzer; the energy scale of the analyzer was calibrated using a clean gold foil. All the spectra presented here were taken at room temperature with a photon energy of 1840 eV. The base pressure in the UHV experimental chamber was in the low 10^{-9} mbar range. The pellets were thoroughly scraped with a diamond file to remove the surface contamination. The core level Fe 2p and Mo 3p spectra presented here are new, whereas the valence band spectrum was already presented in a previous study.[21]

3 Calculation details

The electronic structure of Sr_2FeMoO_6 was calculated using a double cluster model, composed by an FeO_6 and a MoO_6 octahedra sharing a corner O atom. The double octahedra considered here is represented schematically in the top panel of Fig. 1. The double cluster model was solved using a symmetry-adapted configuration interaction method.[16,18] The Fe 3d and Mo 4d orbitals are split by crystal field effects into t_{2g} and e_g symmetries. The symmetry-adapted combination of orbitals with a local t_{2g} and e_g character are depicted in the bottom panel of Fig. 1. The t_{2g} combination is crucial to describe the minority Fe–O–Mo delocalized electron, which is related to both the half-metallic and ferrimagnetic character of Sr_2FeMoO_6.

In a first ionic approximation, the transition metals ions in Sr_2FeMoO_6 are in a $3d^54d^1$ state.[22] The ground state is expanded in terms of $3d^{5+n}\underline{L}^{n+m}4d^{1+m}$ covalently mixed configurations, where $\underline{L}$ denotes a symmetry-adapted O 2p ligand hole. All the possible charge transfer configurations are included explicitly in the ground state expansion. Non-local charge fluctuations such as $3d^54d^1 \rightarrow 3d^44d^2$ and $3d^54d^1 \rightarrow 3d^64d^0$ are also contemplated. They can be achieved by an indirect second-order process via the O 2p orbitals, for instance: $3d^54d^1 \rightarrow 3d^6\underline{L}4d^1 \rightarrow 3d^64d^0$.

There are two complete sets of model parameters for each transition metal octahedron: the Coulomb repulsion U, the p–d charge transfer energy Δ, the core-hole potential Q ($Q = U/0.83$), and the pdσ charge transfer integral T_σ ($T_\pi = -T_\sigma/2$).[17] These parameters are given with respect to the average of the multiplet of each configuration. The multiplet splittings of each $3d^{5+n}\underline{L}^{n+m}4d^{1+m}$ charge transfer configuration are given in terms of the crystal field parameter $10Dq$, the set of Kanamori parameters u, u', and j, as well as the p–p hybridization $pp\sigma$–$pp\pi$.[17] The main model parameters and the multiplet parameters for the FeO_6 and MoO_6 octahedra are given in Table 1. These parameters follow the expected chemical trend,[17,18] and are consistent with those in related compounds.[22–24]

The calculation of the different spectral weights is performed in three steps. First, the Hamiltonian matrix $\hat{H}$ is diagonalized to obtain the ground state $|\psi_0\rangle$. Then, the corresponding Green function $G(\omega)$ is calculated using the following expression:

$$G(\omega) = \left\langle \psi_0 \left| \hat{O}^\dagger \frac{1}{\omega - \hat{H} + i\Gamma/2} \hat{O} \right| \psi_0 \right\rangle,$$

where $\hat{O}$ is the appropriate operator for each experimental technique. For the valence band photoemission spectrum, $\hat{O}$ annihilates the Fe 3d, Mo 4d and O 2p valence electrons. For the core level photoemission spectra, $\hat{O}$ annihilates Fe 2p and Mo
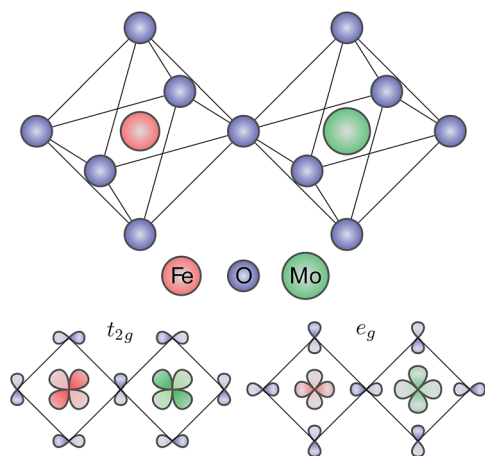

Fig. 1 Schematic representation of the octahedra used in the double cluster model calculation (top panel). Schematic representation of the symmetry-adapted combinations of orbitals with local t_{2g} and e_g characters (bottom panel).

Table 1 Model parameters used in the double cluster calculation. The main parameters are: the Coulomb repulsion U, the p–d charge transfer energy Δ, and the pdσ charge transfer integral T_σ. The multiplet parameters are: the crystal field parameter $10Dq$, the exchange interaction j, and the $pp\sigma$–$pp\pi$ hybridization. All values are given in eV

Parameter	Fe^{3+}	Mo^{5+}
U	7.5	2.6
Δ	3.0	6.1
T_σ	2.1	3.9
$10Dq$	1.3	3.3
j	0.8	0.6
$pp\sigma$–$pp\pi$	1.0	1.0

3p core electrons. Finally, the corresponding spectral weight function $A(\omega)$ is obtained using the standard formula:

$$A(\omega) = -\frac{1}{\pi} \, \text{Im} \, G(\omega),$$

The entire calculation procedure is implemented using the built in facilities of the Quanty package.[25–27] The single cluster model calculations of the FeO_6 and MoO_6 octahedra were performed in the same way and using the same set of parameters.

4   Results and discussion

4.1   Ground state properties

The occupancy of the different configuration in the ground state of Sr_2FeMoO_6 are listed in Table 2. The dominant contribution is given by the charge transfer configurations $3d^5\underline{L}4d^2$ and $3d^6\underline{L}4d^1$, which are followed by the base ionic configuration $3d^54d^1$. The relatively large occupancy of the charge transfer configurations indicates a great degree of covalent bonding. The calculated occupation of the Fe 3d orbitals in the ground state is 5.5 electrons, whereas the calculated occupation of the Mo 4d levels is 1.6 electrons. These occupations are larger than the expected Fe^{3+} ($3d^5$) and Mo^{5+} ($4d^1$) ionic values, which signals the importance of the Fe 3d–O 2p and Mo 4d–O 2p hybridization. The relevance of hybridization is also revealed by the relatively large occupancy of the double charge transfer configuration $3d^6\underline{L}^24d^2$.

The relatively large percentage of the $3d^64d^0$ configuration indicates the importance of non-local Mo–O–Fe charge fluctuations. This configuration is not achieved by the direct $3d^54d^1 \rightarrow 3d^64d^0$ process, but rather by the indirect $3d^54d^1 \rightarrow 3d^6\underline{L}4d^1 \rightarrow 3d^64d^0$ process. On the other hand, the opposite non-local Fe–O–Mo charge transfer $3d^44d^2$ configuration shows a relatively small occupation. This charge fluctuation is strongly suppressed due to the relatively large exchange stabilization of the Fe $3d^5$ electrons. It is worth noting that the relatively strong $3d^54d^1 \rightarrow 3d^64d^0$ process corresponds to the minority Mo $4d^1$ electron, whereas the $3d^54d^1 \rightarrow 3d^44d^2$ transition involves the majority Fe $3d^5$ electrons and is greatly diminished. The

opposite behavior of the minority vs. majority charge fluctuations is in agreement with the half-metallic character of Sr_2FeMoO_6.

4.2   Fe 2p core level spectroscopy

Fig. 2 shows the experimental Fe 2p core level photoemission spectrum of Sr_2FeMoO_6 (dots). The Fe 2p peak is split by spin–orbit interaction into the Fe $2p_{3/2}$ and Fe $2p_{1/2}$ contributions about 711 and 724 eV, respectively. In turn, these peaks are followed by broad charge transfer satellites at around 718 eV and 731 eV.

Fig. 2 also compares the experimental result to the calculated core level spectral weight (solid line). The top panel displays the results of the double cluster calculation, whereas the bottom panel compares to the single cluster model results. The discrete contributions were broadened with Gaussian and Lorentzian broadenings to account for the experimental resolution and the
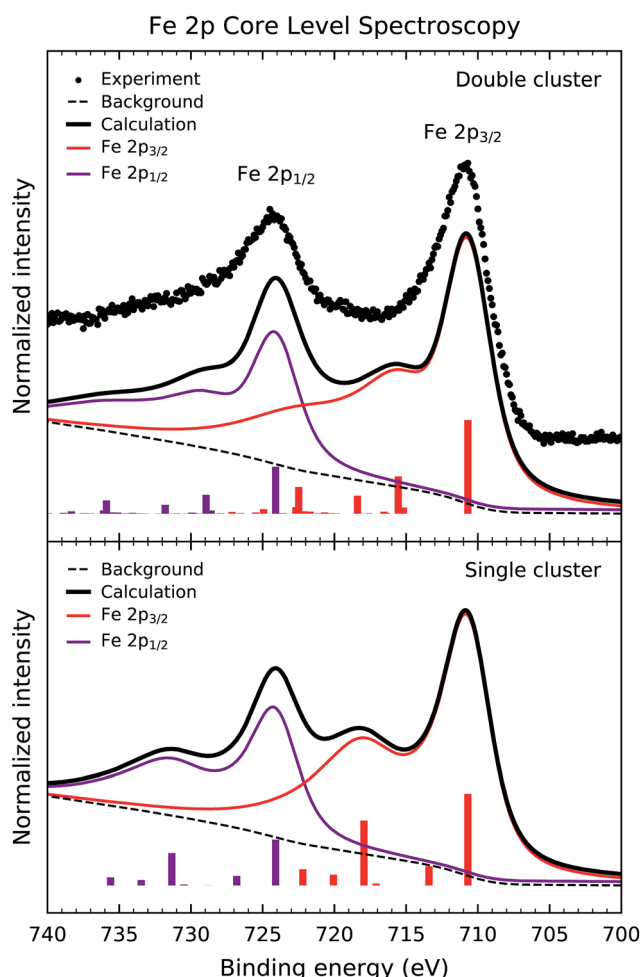

Fig. 2 Fe 2p core level photoemission spectrum of Sr_2FeMoO_6 (dots) compared to the calculated spectral weight (solid line) of the double and single cluster models. The experimental spectrum presents the Fe $2p_{3/2}$ and Fe $2p_{1/2}$ components and the respective charge transfer satellites. The calculated spectrum is dominated by well screened Fe $2p^53d^6\underline{L}$ states and exhibits satellite structures of Fe $2p^53d^7\underline{L}^2$ character.

Table 2 Occupancy of the different configurations in the calculated ground state of Sr_2FeMoO_6

Configuration	Occupancy
$3d^5\underline{L}4d^2$	20.9%
$3d^6\underline{L}4d^1$	20.0%
$3d^54d^1$	19.6%
$3d^6\underline{L}^24d^2$	15.2%
$3d^5\underline{L}^24d^3$	7.7%
$3d^64d^0$	7.3%
$3d^6\underline{L}^34d^3$	4.8%
$3d^5\underline{L}^34d^4$	1.3%
$3d^7\underline{L}^24d^1$	1.2%
$3d^7\underline{L}^34d^2$	0.7%
$3d^6\underline{L}^44d^4$	0.7%
$3d^7\underline{L}4d^0$	0.5%
$3d^44d^2$	0.1%

core hole lifetime. Finally, an integral background was added to the calculated curve to take into account inelastic processes.

The calculated spectral weight of the double cluster model reproduces satisfactorily the experimental data. The main peaks are due to the well screened Fe $2p^5 3d^6 \underline{L}$ states, whereas the satellite structures are composed of Fe $2p^5 3d^7 \underline{L}^2$ states. These charge transfer satellites in the core level spectrum represent a many-body effect, which reflects the highly correlated nature of the Fe^{3+} ($3d^5$) ion in Sr_2FeMoO_6 ($U > T_\sigma$). The energy position and relative intensity of the satellites are sensitive to the U, Δ and T_σ parameters. On the other hand, the single cluster calculation overestimates the intensity of the charge transfer satellites, mainly because it does not include the non-local screening contribution which comes from the MoO_6 octahedra.

4.3 Mo 3p core level spectroscopy

Fig. 3 shows the experimental Mo 3p core level photoemission spectrum of Sr_2FeMoO_6 (dots). The Mo 3p peaks are split by
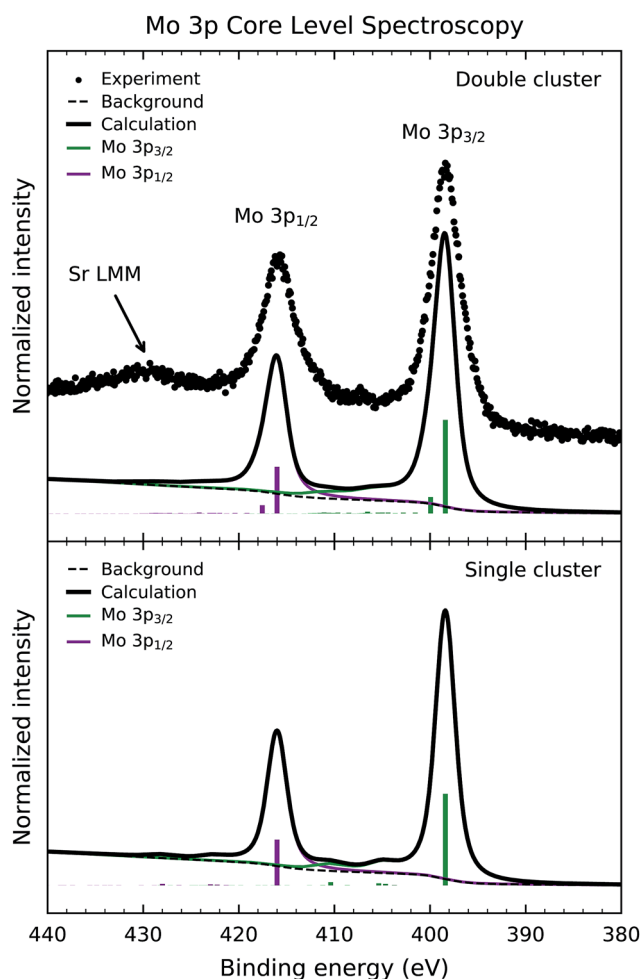

Fig. 3 Mo 3p core-level photoemission spectrum of Sr_2FeMoO_6 (dots) compared to the calculated spectral weight (solid line) of the double and single cluster models. The experimental spectrum presents the Mo $3p_{3/2}$ and Mo $3p_{1/2}$ peaks, while the structure around 430 eV is due to Sr LMM Auger decay. The calculated spectrum is dominated by states with Mo $3p^5 4d^1$ character.

spin–orbit interaction into the Mo $3p_{3/2}$ and Mo $3p_{1/2}$ contributions around 398 and 416 eV, respectively. In this case, the core level spectrum does not exhibit a prominent satellite structure. Finally, the experimental data presents an accidental superposition with the Sr LMM Auger electron decay around 430 eV.

Fig. 3 also compares the experimental data to the calculated core-level spectral weight (solid line) of the double and single cluster models. Likewise, the discrete contributions were also broadened to account for the experimental resolution and the core hole lifetime. In the same way, the integral background was calculated and added to the final calculated curve.

The calculated spectral weight of the double cluster calculation successfully reproduces the peaks in the experimental result. The leading structure at 398 eV arises from mixed Mo $3p^5 4d^2 \underline{L}$ and $3p^5 4d^1$ final states, while the smaller contribution at 400 eV has mainly Mo $3p^5 4d^1$ character. The smaller satellite structure, in this case, is attributed to the less correlated character of the Mo^{5+} ($4d^1$) ion in Sr_2FeMoO_6 ($U < T_\sigma$). For this reason, the calculated results are less sensitive to the values of the model parameters. In this case, the single cluster calculation reproduces reasonably well the experimental spectrum, mainly because the charge transfer processes are less important than in the Fe 2p core level spectrum.

4.4 Valence band spectroscopy

Fig. 4 presents the experimental valence band photoemission spectrum of Sr_2FeMoO_6 (dots). The dashed line denotes the Fermi level energy E_F. The spectrum is composed of three main regions: the Fe 3d–O 2p–Mo 4d mixed states close to the Fermi level, the non-bonding and bonding O 2p band from 9 to 4 eV, and the Fe 3d charge transfer satellites from 15 to 9 eV.

Fig. 4 also compares the experimental data to the calculated spectral weight (solid line) using double and single cluster model calculations. The individual contributions of the Fe 3d, Mo 4d and O 2p states are presented below. The intensity of the peaks were weighted with the appropriate photoelectron cross-sections for a photon energy of 1840 eV. The discrete peaks were convoluted with a Gaussian function to account for the experimental resolution. Finally, an integral background was added to take into account inelastic scattering effects. The single cluster result was calculated using a linear combination of the FeO_6 and MoO_6 single clusters.

The calculated spectral weight of the double cluster model is in good agreement with the experimental valence band photoemission data. The first feature around 1.0 eV is attributed to Fe 3d–O 2p–Mo 4d mixed states; these are related to the non-local charge fluctuations which give rise to the conducting behavior of Sr_2FeMoO_6. The Fe 3d states are split by crystal field effects into the Fe t_{2g} and Fe e_g contributions, and appear about 5.5 and 4.0 eV, respectively. The non-bonding O 2p band corresponds to O 2p states which are not hybridized with Fe 3d and Mo 4d states, and shows up between 4.0 and 8.0 eV (purple line). On the other hand, the bonding O 2p band corresponds to O 2p states which are hybridized with Fe 3d and Mo 4d states, and arises from 6.0 and 10.0 eV (blue line). Finally, the charge
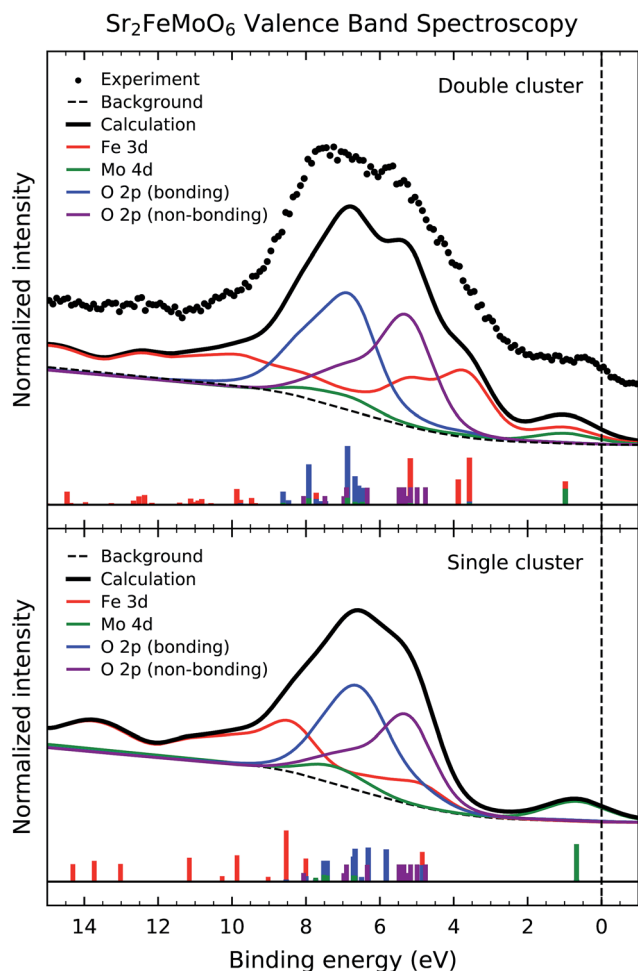
Sr$_2$FeMoO$_6$ Valence Band Spectroscopy

Fig. 4 Valence band photoemission spectrum of Sr$_2$FeMoO$_6$ (dots) compared to the calculated spectral weight (solid line) of the double and single cluster models. The experimental spectrum is composed of Fe 3d–O 2p–Mo 4d mixed states close to the Fermi level, non-bonding and bonding O 2p band from 9 to 4 eV, and the Fe 3d charge transfer satellites from 15 to 9 eV. The first feature around 1 eV is attributed to Fe 3d–O 2p–Mo 4d mixed states, while the bottom of the valence band is dominated by charge transfer satellites related to the Fe 3d states.

compound. The double cluster model gives an anti-parallel ordering of the Fe 3d^5 and Mo 4d^1 magnetic moments, which is in agreement with the observed ferrimagnetic ordering in Sr$_2$FeMoO$_6$, whereas the single cluster model produces an independent alignment of the magnetic moments yielding a paramagnetic state. Further, the double cluster model indicates the importance of the non-local Fe 3d–O 2p–Mo 4d fluctuations, which are related to the half-metallic character of this oxide, whereas the single cluster model only consider the local Fe 3d–O 2p and Mo 4d–O 2p fluctuations and gives rise to an insulating state.

The non-local charge fluctuations are reflected not only in the composition of the ground state, but also contribute to the individual transitions in the experimental spectra. In fact, the first removal state in the valence band spectra, around 1 eV, is a non-local Fe 3d–O 2p–Mo 4d mixed state, according to the double cluster, but it is a local Mo 4d–O 2p state in the single cluster calculation. Therefore, the double cluster calculation is crucial to explain not only the physical properties of Sr$_2$FeMoO$_6$, but also the character of the spectral features present in the valence band spectrum.

5 Summary and conclusions

In summary, we studied the electronic structure of Sr$_2$FeMoO$_6$ using bulk sensitive photoemission spectroscopy. The experimental data were analyzed using configuration interaction cluster model calculations. The charge transfer 3d^5$\underline{L}$4d^2 and 3d^6$\underline{L}$4d^1 configurations dominate the ground state; this indicates a large degree of Fe–O and Mo–O hybridization in this compound. The occupancy of the 3d^{6}4d^0 configuration shows the importance of non-local Fe–O–Mo charge fluctuations; this configuration is achieved through the indirect 3d^{5}4d^1 → 3d^6$\underline{L}$4d^1 → 3d^{6}4d^0 process. This non-local charge fluctuation occurs in the minority spin channel, whereas the transitions in the majority spin sector are strongly suppressed; which is in accordance with the half-metallic character attributed to the Sr$_2$FeMoO$_6$ compound. The Fe 2p core level photoemission spectrum shows rather large charge transfer satellites. These satellites are related to many-body effects caused by the highly correlated nature of the Fe 3d levels. On the other hand, these effects are smaller in the Mo 3p core level spectrum due to the less correlated character of the Mo 4d states. Charge transfer satellites are also observed in the valence band spectrum and are again associated to the Fe 3d electrons. Although the single cluster model calculations are able to reproduce the experimental spectra, they fail to explain the physical properties of the Sr$_2$FeMoO$_6$ compound. In this context, the double cluster model calculations are crucial to explain both the ferrimagnetic ordering and the half-metallic character of this compound. To conclude, the metal–oxygen hybridization, non-local Fe–O–Mo charge fluctuations, and many-body effects are all relevant topics in the electronic structure of Sr$_2$FeMoO$_6$.

Conflicts of interest

There are no conflicts to declare.

transfer satellites, mostly related to the Fe 3d states, emerge above 9.0 eV. We note that the Fe 3d–O 2p and Mo 4d–O 2p hybridization are crucial to describe the features in the valence band spectrum. Further, the correlation effects of the Fe 3d states is essential to explain the charge transfer satellites at high binding energies.

The Mo 4d spectral weight (green line) presents a peak around 1.0 eV as well as structure about 8.0 eV. The former is related to the Fe 3d–O 2p–Mo 4d mixed states, whereas the later is attributed to Mo 4d–O 2p hybridization. The energy position and relative intensity of these Mo 4d structures are in agreement with those observed in a recent Mo L$_3$ resonant photoemission experiment.[21]

Although the single cluster model results reproduce the overall shape of the valence band, they fail to explain the magnetic order and the electrical conductivity of the

Acknowledgements

References

1 K.-I. Kobayashi, T. Kimura, H. Sawada, K. Terakura and Y. Tokura, *Nature*, 1998, **395**, 677–680.

2 Y. Tomioka, T. Okuda, Y. Okimoto, R. Kumai, K.-I. Kobayashi and Y. Tokura, *Phys. Rev. B*, 2000, **61**, 422–427.

3 L. Balcells, J. Navarro, M. Bibes, A. Roig, B. Martínez and J. Fontcuberta, *Appl. Phys. Lett.*, 2001, **78**, 781–783.

4 A. Gupta and J. Z. Sun, *J. Magn. Magn. Mater.*, 1999, **200**, 24–43.

5 M. Ziese, *Rep. Prog. Phys.*, 2002, **65**, 143.

6 D. Serrate, J. M. De Teresa, P. A. Algarabel, C. Marquina, J. Blasco, M. R. Ibarra and J. Galibert, *J. Phys.: Condens. Matter*, 2007, **19**, 436226.

7 D. D. Sarma, P. Mahadevan, T. Saha-Dasgupta, S. Ray and A. Kumar, *Phys. Rev. Lett.*, 2000, **85**, 2549–2552.

8 M. S. Moreno, J. E. Gayone, M. Abbate, A. Caneiro, D. Niebieskikwiat, R. D. Sánchez, A. de Siervo, R. Landers and G. Zampieri, *Solid State Commun.*, 2001, **120**, 161–164.

9 K. Kuepper, I. Balasz, H. Hesse, A. Winiarski, K. C. Prince, M. Matteucci, D. Wett, R. Szargan, E. Burzo and M. Neumann, *Phys. Status Solidi A*, 2004, **201**, 3252–3256.

10 T. Saitoh, M. Nakatake, A. Kakizaki, H. Nakajima, O. Morimoto, S. Xu, Y. Moritomo, N. Hamada and Y. Aiura, *Phys. Rev. B: Condens. Matter Mater. Phys.*, 2002, **66**, 035112.

11 J.-S. Kang, J. H. Kim, A. Sekiyama, S. Kasai, S. Suga, S. W. Han, K. H. Kim, T. Muro, Y. Saitoh, C. Hwang, C. G. Olson, B. J. Park, B. W. Lee, J. H. Shim, J. H. Park and B. I. Min, *Phys. Rev. B: Condens. Matter Mater. Phys.*, 2002, **66**, 113105.

12 J. Navarro, J. Fontcuberta, M. Izquierdo, J. Avila and M. C. Asensio, *Phys. Rev. B: Condens. Matter Mater. Phys.*, 2004, **69**, 115101.

13 S. Ray, A. Kumar, D. D. Sarma, R. Cimino, S. Turchini, S. Zennaro and N. Zema, *Phys. Rev. Lett.*, 2001, **87**, 097204.

14 K. Kuepper, M. Kadiroglu, A. V. Postnikov, K. C. Prince, M. Matteucci, V. R. Galakhov, H. Hesse, G. Borstel and M. Neumann, *J. Phys.: Condens. Matter*, 2005, **17**, 4309–4317.

15 M. Besse, V. Cros, A. Barthélémy, H. Jaffrès, J. Vogel, F. Petroff, A. Mirone, A. Tagliaferri, P. Bencok, P. Decorse, P. Berthet, Z. Szotek, W. M. Temmerman, S. S. Dhesi, N. B. Brookes, A. Rogalev and A. Fert, *Europhys. Lett.*, 2002, **60**, 608–614.

16 G. van der Laan, C. Westra, C. Haas and G. A. Sawatzky, *Phys. Rev. B*, 1981, **23**, 4369–4380.

17 A. E. Bocquet, A. Fujimori, T. Mizokawa, T. Saitoh, H. Namatame, S. Suga, N. Kimizuka, Y. Takeda and M. Takano, *Phys. Rev. B: Condens. Matter Mater. Phys.*, 1992, **45**, 1561–1570.

18 M. Imada, A. Fujimori and Y. Tokura, *Rev. Mod. Phys.*, 1998, **70**, 1039–1263.

19 E. B. Guedes, M. Abbate, K. Ishigami, A. Fujimori, K. Yoshimatsu, H. Kumigashira, M. Oshima, F. C. Vicentin, P. T. Fonseca and R. J. O. Mossanek, *Phys. Rev. B: Condens. Matter Mater. Phys.*, 2012, **86**, 235127.

20 M. Abbate, F. C. Vicentin, V. Compagnon-Cailhol, M. C. Rocha and H. Tolentino, *J. Synchrotron Radiat.*, 1999, **6**, 964–972.

21 H. P. Martins, F. Prado, A. Caneiro, F. C. Vicentin, R. J. O. Mossanek and M. Abbate, *Europhys. Lett.*, 2017, **118**, 37002.

22 H. P. Martins, F. Prado, A. Caneiro, F. C. Vicentin, D. S. Chaves, R. J. O. Mossanek and M. Abbate, *J. Alloys Compd.*, 2015, **640**, 511–516.

23 M. Abbate, G. Zampieri, J. Okamoto, A. Fujimori, S. Kawasaki and M. Takano, *Phys. Rev. B: Condens. Matter Mater. Phys.*, 2002, **65**, 165120.

24 V. Stoeberl, M. Abbate, L. M. S. Alves, C. A. M. dos Santos and R. J. O. Mossanek, *J. Alloys Compd.*, 2017, **691**, 138–143.

25 M. W. Haverkort, M. Zwierzycki and O. K. Andersen, *Phys. Rev. B: Condens. Matter Mater. Phys.*, 2012, **85**, 165113.

26 M. W. Haverkort, G. Sangiovanni, P. Hansmann, A. Toschi, Y. Lu and S. Macke, *Europhys. Lett.*, 2014, **108**, 57004.

27 Y. Lu, M. Höppner, O. Gunnarsson and M. W. Haverkort, *Phys. Rev. B: Condens. Matter Mater. Phys.*, 2014, **90**, 085102.